A Simplified Prediction of Gear Currents Propagation in EV Drivetrains Using a Conductive Susceptibility Framework

Results in Engineering 32 (2026) 111934

Contents lists available at ScienceDirect

Results in Engineering

journal homepage: www.sciencedirect.com/journal/results-in-engineering

Research paper

Simplified Prediction of Gear Currents Propagation in EV Drivetrains Using a Conductive Susceptibility Framework

Leonardo I. Farfan-Cabrera [a,*], Renato Galluzzi [a], Andys Hernández-Peña [a], Thomas Tobie [b]

[a] Tecnologico de Monterrey, School of Engineering and Sciences, Ave. Eugenio Garza Sada 2501, Monterrey, 64700, Mexico
[b] School of Engineering and Design, Gear Research Center (FZG), Technical University of Munich, Garching bei München, 85748, Germany

A R T I C L E I N F O

Keywords:
Electric vehicle
Bearing current
Shaft voltage
Drivetrain
Gear

A B S T R A C T

Stray electrical currents generated in electric motors are a reliability concern in electric vehicle (EV) drivetrains, as they can promote premature tribological failures. Most existing studies focus on bearing currents assuming that bearings are the primary discharge paths to ground during stray current events. However, EV drivetrains combine electric motors with multi-stage gear transmissions, introducing additional lubricated contacts that may contribute to critical failures during operation. The potential involvement of gear contacts in stray current phenomena has received little attention, partly due to the complexity of electrified drivetrains and the insufficient maturity of the topic. This work proposes a simplified predictive methodology toward identifying operating conditions under which gear contacts in EV drivetrains may become susceptible to conduct or discharge stray currents (gear currents). The occurrence and propagation of these currents along the drivetrain can be a potential failure risk since electrically assisted surface degradation may promote accelerated wear and unexpected efficiency loss situations. The study framework combines operating conditions derived from a common driving cycle, elastohydrodynamic lubrication simulations, and a simplified resistive network linking tribological behavior with electrical conduction. It is applied to a two-stage EV drivetrain by considering two different study cases of surface roughness conditions for bearings and gears. The results show that conductive paths are highly dependent on operating conditions and lubrication regimes. Gear meshes exhibited significant conductive susceptibility and frequently participated in dominant current paths under typical roughness values for gears. In contrast, smoother gear surfaces improved lubrication separation and shift current propagation toward bearings.

1. Introduction

The rapid electrification of the transportation sector has led to a widespread adoption of electric vehicles (EVs). Compared with conventional internal combustion engine drivetrains, electric drivetrains exhibit a different set of operating characteristics, including much higher rotational speeds (>10,000 rpm), faster torque transients, and the integration of a power electronics module that controls the electric motor for the variable and demanding driving conditions [1]. While these features enable improved performance and efficiency for the EV, they also introduce new reliability challenges that are not present in traditional internal combustion engine drivetrains. Among these challenges, the occurrence of shaft voltages and stray electrical currents has emerged as an important tribological concern affecting the durability of rolling bearings [2–4]. Shaft voltages in electric machines are mainly generated by the switching behavior of inverter-driven motors, which induces high-frequency voltages between the rotor of the electric machine and its grounded housing. When this potential exceeds the dielectric strength of lubricated interfaces in the drivetrain, discharge events may occur through conductive paths mainly linked to rolling bearings and gears. These events, often named as bearing currents, are known to cause different damages to the bearings (i.e., electrical discharge machining (EDM) damage, surface pitting, lubricant degradation, and accelerated fatigue) [4–6]. As EV drivetrains continue to increase in power density and inverter switching frequency, the failure risks and technological solutions associated with shaft voltage phenomena become a more significant active topic of research in both academia and industry. Additionally, the complexity of shaft voltage dynamics, especially the way it interacts with lubricated interfaces, makes it a challenging issue for EV manufacturers to fully understand and solve the related problems.

Most existing investigations on stray currents in electrified

* Corresponding author.
E-mail address: farfanl@tec.mx (L.I. Farfan-Cabrera).

https://doi.org/10.1016/j.rineng.2026.111934
Received 21 May 2026; Received in revised form 27 June 2026; Accepted 9 July 2026
Available online 10 July 2026

drivetrains have exclusively focused on bearing current mechanisms, implicitly assuming that rolling bearings constitute the primary discharge path between the motor shaft and the housing [4–11]. Even though, significant efforts have been made in developing simulation tools to assess and predict the tribological behavior alteration in bearings due to electrical inducements, evidencing the complexity and detrimental effects for the drivetrain [12–17]. However, modern EV drivetrains not only involve bearings, but they also typically incorporate multi-stage reduction gearboxes that operate under a shared lubrication system and contain multiple lubricated contact interfaces, including gear meshes [18,19]. Under the highly variable operating conditions of an EV, all the lubricated interfaces can create different conductive paths for stray currents in the drivetrain, allowing them to pass through bearings and/or gears before reaching ground. This behavior depends strongly on the instantaneous lubrication regime and the dielectric strength present in each tribological contact during operation. In mixed or boundary lubrication, direct asperity contact facilitates electrical conduction, whereas in hydrodynamic lubrication, the lubricant film can act as a strong dielectric layer, increasing electrical resistance and limiting current passing. As a result, leakage currents can travel differently through the drivetrain and, under certain conditions, interact with gear contacts, potentially causing electro-tribological damaging effects in both bearings and gears.

As EV drivetrains continue to evolve in complexity, the role of gear contacts in stray-current phenomena remains relatively underexplored as compared to solely bearing failures. The main reasons for this knowledge gap are related to the limited and restricted data provided by car makers and original equipment manufacturers in terms of wear, fatigue and failure modes of automotive components. Additionally, the elevated multiphysical complexity of the interplay between transient lubrication behavior and electrical conduction mechanisms across multiple drivetrain components and operating conditions plays a major role. As a reference, even the precise calculation of a single isolated electrical resistance/impedance of a lubricated contact can be very challenging since it varies depending on factors such as operating conditions, surface roughness, lubricant properties, and asperity interactions [20], making fully predictive electro-tribological modeling of more complex electrified tribo-systems, such as EV drivetrains, particularly challenging [21].

To address this challenge, simplified system-level approaches capable of identifying susceptible operating conditions and conductive pathways are currently needed, particularly during early drivetrain design stages. For example, recent studies have emphasized the importance of methodologies to analyze the lubrication behavior in high-speed EV reducers, not only from the perspective of efficiency but also as a critical factor governing tribological reliability. Jia et al. [22] demonstrated through smoothed particle hydrodynamics (SPH) simulations and experimental validation that lubricant distribution within EV reducers is highly dependent on operating conditions and gearbox orientation, directly influencing the lubrication quality of bearings and gears. Their findings showed that insufficient lubricant supply can lead to unstable lubrication conditions, particularly in certain bearing locations, while excessive lubricant increases churning losses and reduces drivetrain efficiency. These results reinforce the need to better understand lubrication dynamics in EV transmissions, as variations in film formation may not only affect efficiency and wear, but also alter the electrical insulation behavior of lubricated contacts under stray-current conditions.

Hence, this research proposes a pioneer simulation-based framework to predict the conductive susceptibility of EV drivetrains, with emphasis on potential leakage-current propagation through gear meshes. The present methodology combines drivetrain operating conditions derived from a representative driving cycle, tribological lubrication simulations of bearings and gear meshes, and a simplified electrical network representation of the drivetrain. This simplified approach allows the identification of conductive paths and the estimation of the likelihood of current propagation through drivetrain tribological interfaces by linking the lubrication regime transitions to equivalent electrical resistances. The framework is implemented for a representative EV drivetrain that consists of an electric motor coupled to a two-stage reduction gearbox using operating conditions derived from the worldwide light-duty test cycle (WLTC) class 3 cycle [23], as well as elastohydrodynamic lubrication simulations to determine film thickness and lubrication regimes for the different scenarios. Two study cases were investigated to evaluate the influence of surface roughness of bearings and gears on the predicted conductive susceptibility in order to exemplify the proposed methodology.

2. Methodology

The methodology followed in this study integrates a drivetrain operating analysis, lubrication simulation, and a simplified electrical representation to evaluate the conductive susceptibility of a common EV drivetrain. The implemented framework workflow is shown in Fig. 1. Firstly, representative operating conditions are derived from a transient driving cycle by converting vehicle speed into motor torque and speed through a backward vehicle model. The resulting torque–speed history is then discretized into a reduced set of 25 representative operating scenarios using a clustering approach. These operating points are used as inputs for drivetrain simulations. Elastohydrodynamic lubrication (EHL) simulations are conducted for all bearings and gear meshes to obtain the corresponding minimum lubricant film thickness for each scenario. The lubrication state of each interface is subsequently characterized through the corresponding lambda ratio, which provides an indicator of the separation between contacting surfaces. The tribological information obtained is then incorporated into a conductive susceptibility scheme (CSS), where the drivetrain is represented as a simplified resistive network. This simplified framework enables the identification of possible conductive paths, the estimation of dominant grounding locations, and the evaluation of the likelihood of gear-current propagation. Finally, the scenario-based results are aggregated using duty-cycle weighting from the WLTC to obtain operation-representative indicators of conductive susceptibility in the drivetrain.

2.1. EV drivetrain architecture and operating conditions

The two-stage parallel-axis drivetrain illustrated in Fig. 2 was selected for the aim of this study. While this model is available as a template in KISSsoft's library, it matches the transmission requirements of most vehicles in the C-class vehicle segment. The illustrated system consists of the electric motor shaft supported by deep groove ball bearings b_1 to b_4, an intermediate shaft supported by deep groove ball bearings b_5 and b_6, an output shaft supported by tapered roller bearings b_7 and b_8, as well as two gear meshes: z_1z_2 (input or first stage), and z_3z_4 (output or second stage). Both gear pairs are helical; they yield together a total transmission ratio $i = \frac{671}{78} \cong 8.6$. This parameter falls within the values expected for most single-speed EVs.

The voltage source V_s representing shaft voltage excitation is assumed to be located on the motor shaft between bearings b_1 and b_2. This location reflects typical EV shaft voltage generation mechanisms originating at the motor rotor. It is considered that all bearings and gear meshes operate under a common lubrication system (using the same lubricant) within this drivetrain model and are subjected to torque-dependent contact loading and speed-dependent entrainment conditions.

The operating conditions considered for the EV drivetrain were derived from a backward longitudinal model of a C-class vehicle with parameters found in literature [23]. The model was simulated with a time step of 0.5 s while fed by the WLTC class 3 driving cycle. Results in terms of electric motor torque, electric motor speed and vehicle speed are plotted in Fig. 3. The driving cycle spans 30 minutes (1800 s) and

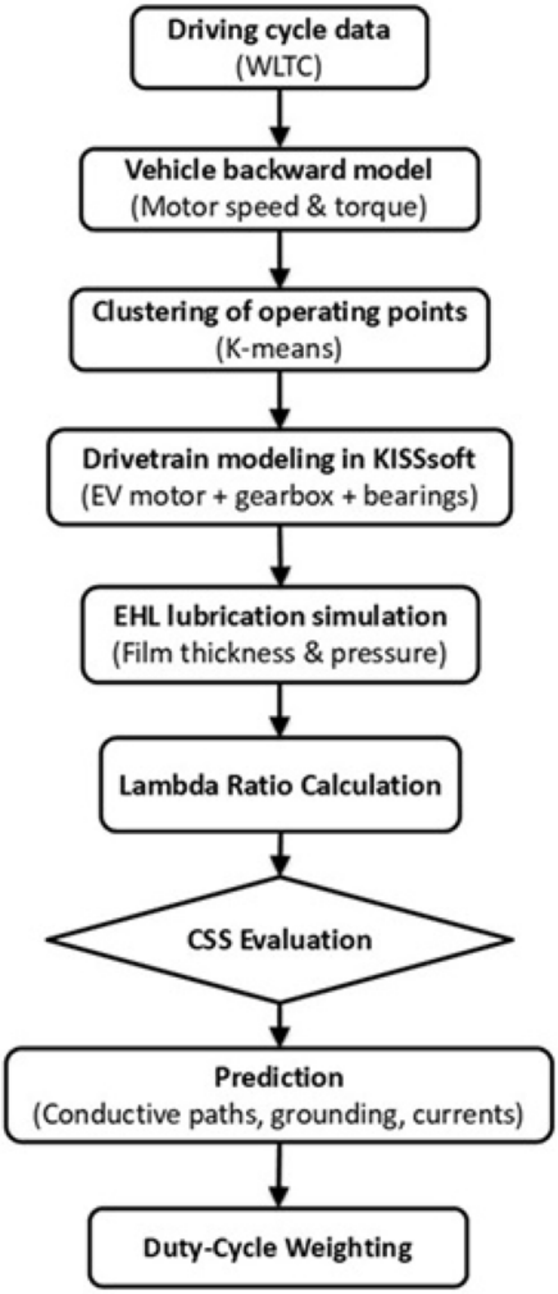

Fig. 1. Overall methodology of the study.

includes low-speed urban operation, repeated acceleration and deceleration events, regenerative braking phases (negative torque and positive angular speed), and high-speed steady-state portions. Motor speed varies from near standstill up to approximately 9000 rpm, while torque ranges from about −100 Nm to +150 Nm. To enable the lubrication parameters analysis in the software, the continuous time histories of speed and torque were discretized into representative operating points defined by $T(k)$ for motor torque and $\omega(k)$ for speed. This reduction is necessary, as calculations at each simulated point are impractical due to their computational burden. The extraction of these points was performed with k-means clustering to identify the most representative working conditions in the torque-speed plane. The clustering algorithm aims at partitioning all the points of the driving cycle into a finite set of clusters – 25 in this case – by minimizing all the Euclidean distances of the cycle points within a cluster with respect to a representative point of that cluster. This method is well known to simplify problems for the design of powertrain electric machines [24], as well as mechanical systems for automotive applications [25]. The complete torque–speed points distribution of the cycle is illustrated in Fig. 4. Different colors denote the clusters obtained through k-means; each cluster has a representative point indicated in black. For clarity, the extracted cluster torque–speed points are also listed in Table 1. These representative points were chosen to capture extreme and transitional operating regions, including high-load/low-speed conditions, high-speed/low-load operation, regenerative braking zones, and clusters where lubrication regime transitions are expected in the EV's drivetrain bearings and gears. This reduced but representative subset ensures that the subsequent analysis captures critical minimum film thickness and lubrication regime transitions relevant for the electrically conductive susceptibility assessment.

2.2. Drivetrain modelling and simulation

The minimum film thickness for all lubricated contacts was computed using the commercial software KISSsoft (release 2025), employing its EHL modules for rolling bearings and gear meshes. An ISO-VG 46 mineral oil was adopted as a reference fluid to provide a controlled and generic tribological baseline for the methodology, rather than to represent a specific commercial EV e-fluid formulation. For each selected operating point k, defined by motor speed $\omega(k)$ and torque $T(k)$, the transmitted loads were transmitted through the drivetrain to determine the contact forces acting on bearings b_1–b_8 and gear meshes z_1z_2 and z_3z_4. The corresponding entrainment speeds were calculated from shaft rotational speeds, and steady-state EHL analysis was performed to obtain the minimum film thickness $h_{\min,i}(k)$ for each contact i. The lubrication model accounts for load-dependent contact pressure, lubricant viscosity, material elastic properties, and contact geometry under fully flooded conditions. Surface roughness was incorporated through the composite RMS roughness definition, and lubricant properties were defined at the operating temperature. The specific geometric, material, roughness, and lubricant parameters used in the simulations are summarized in Table 2. These film thickness results constitute the basis for the subsequent analysis of electrically conductive susceptibility classification. Because the proposed analysis is strongly driven by the lambda ratio at the mechanical interfaces, and since lambda is highly sensitive to surface roughness, two study cases were investigated. The first case considers different surface roughness values for bearings and gears, reflecting typical conditions encountered in real drivetrain systems. The second case assumes similar roughness for both bearings and gears, representing an idealized scenario in which all tribological components are manufactured using advanced surface finishing techniques and achieving very low surface roughness.

2.3. Conductive susceptibility scheme (CSS) framework

A conductive susceptibility scheme (CSS) was used as a structured framework to identify drivetrain operating conditions and mechanical interfaces which are susceptible to leakage-current propagation. This approach evaluates the tribological interfaces separation of each lubricated contact through the Lambda ratio as a key role in leakage-current propagation. The Lambda ratio is obtained from the minimum lubricant film thickness and composite surface roughness [26]. Based on the lubrication regime, and assuming that full-film lubrication provides sufficient insulation, the contacts are classified as either electrically insulating or conductive, and assigned corresponding order-of-magnitude electrical resistances. Thus, the drivetrain is represented as a simplified resistive network in which shafts, bearings, and gear meshes are defined as possible conductive paths to the available grounding locations.

The equivalent resistance of these paths is evaluated to identify the dominant conductive route and the most probable discharge ground for

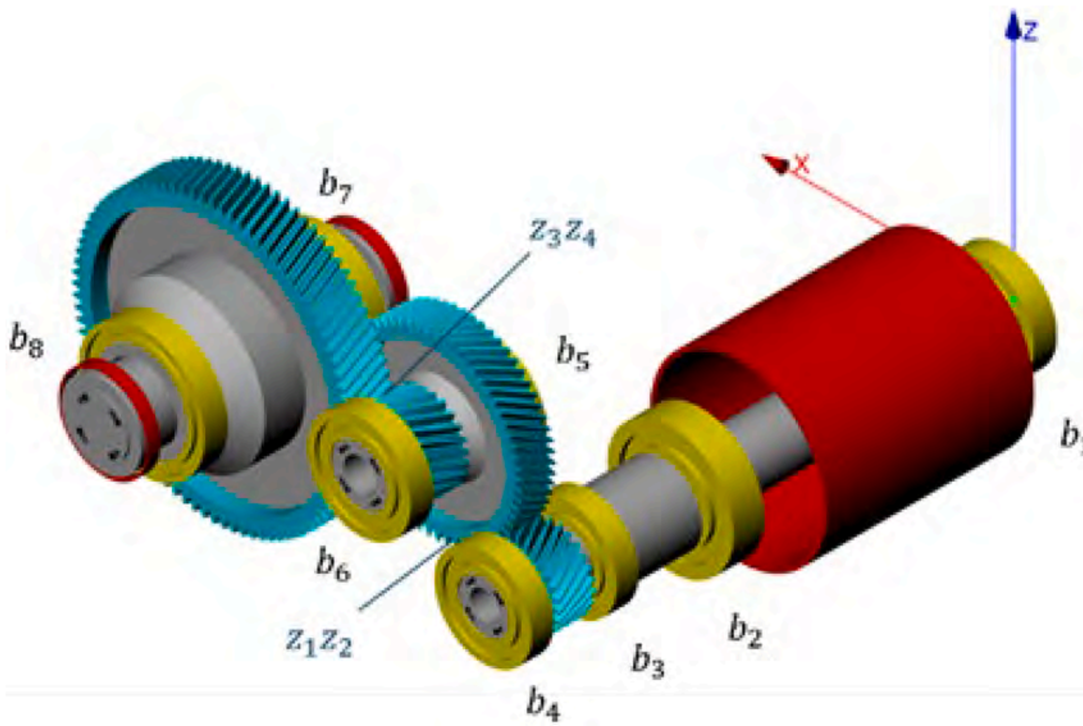

Fig. 2. EV's drivetrain architecture selected for the analysis.

each torque–speed scenario. The normalized conductance of the admissible paths is subsequently used to estimate the relative current distribution and the probability of current propagation through each gear mesh. The drivetrain electrical abstraction used in this analysis is shown in Figs. 5a and 5b. Each ground corresponds to the housing connection of a specific bearing: A–b1, C–b2, D–b3, E–b4, F–b5, G–b6, H–b7, and M–b8. It is important to highlight that a representation merely resistive is intentionally adopted in this study due to the dominant role of lubricated interfaces in conduction continuity. The existence of a conductive path is ultimately governed by whether lubricated contacts allow charge transfer (e.g., via asperity interaction or thin-film conduction). This is captured by the relative resistance of bearings and gear meshes, whereas shaft steel provides an almost lossless conduction backbone.

The drivetrain comprises: Shaft segments modeled as resistances, R_s; Bearing contacts modeled as lubrication-dependent resistances, R_b; Gear meshes modeled as lubrication-dependent resistances, R_z; and a shaft voltage source, V_s, representing inverter-induced excitation.

The electrical resistance of steel shaft segments is several orders of magnitude lower than lubricated contact resistances:

$$R_s \ll R_b, |R_z \tag{1}$$

In the semi-quantitative extension used in this work, finite (but small) shaft resistances are assigned to enable equivalent-resistance computations without altering the dominance of contact impedances.

It is important to note that capacitive effects, dielectric breakdown, and frequency-dependent impedance are not included because the aim of this research is to identify susceptible conductive routes in the drivetrain rather than to predict transient discharge waveforms or switching-frequency phenomena. Future work will be focused on incorporating more complex electrical arrangements and tribological parameters in the modeling.

For each lubricated contact, i, and operating point, k, (torque–speed scenario), the Lambda ratio is computed from the minimum lubricant film thickness, $h_{\min,i}(k)$, and the composite surface roughness, σ_i:

$$\lambda_i(k) = \frac{h_{\min,i}(k)}{\sigma_i} \tag{2}$$

where $h_{\min,i}(k)$ is obtained from the software tribological simulation, and the composite RMS roughness is:

$$\sigma_i = \sqrt{\sigma_{1,i}^2 + \sigma_{2,i}^2} \tag{3}$$

with $\sigma_{1,i}$ and $\sigma_{2,i}$ are the RMS roughness values of the two contacting bodies i (raceway and rolling element for bearings while drive wheel and driven gears for the gear mesh).

The operating-point dependency enters through $h_{\min,i}(k)$, which varies with load, speed, and lubricant viscosity via software computation.

The Lambda ratio is treated as a monotonic indicator of tribological separation and therefore of insulation capability, as expressed:

- Full-film EHL: $\lambda \geq 3$ (predominantly insulating because lubricant is assumed to be dielectric enough to avoid discharge or conduction),
- Mixed lubrication: $1 \leq \lambda < 3$ (potentially conductive due to partial asperities contacts),
- Boundary lubrication: $\lambda < 1$ (highly susceptible because predominant asperities contacts).

Hence, a conservative binary susceptibility indicator may be defined as:

$$S_i(k) = \begin{cases} 1, & \lambda_i(k) < 3 \\ 0, & \lambda_i(k) \geq 3 \end{cases} \tag{4}$$

where $S_i(k) = 1$ denotes an electrically susceptible contact.

For gear meshes, the scenario-level gear susceptibility indicator is:

$$G(k) = \begin{cases} 1, & \exists g : \lambda_{z,g}(k) < 3 \\ 0, & \text{otherwise} \end{cases} \tag{5}$$

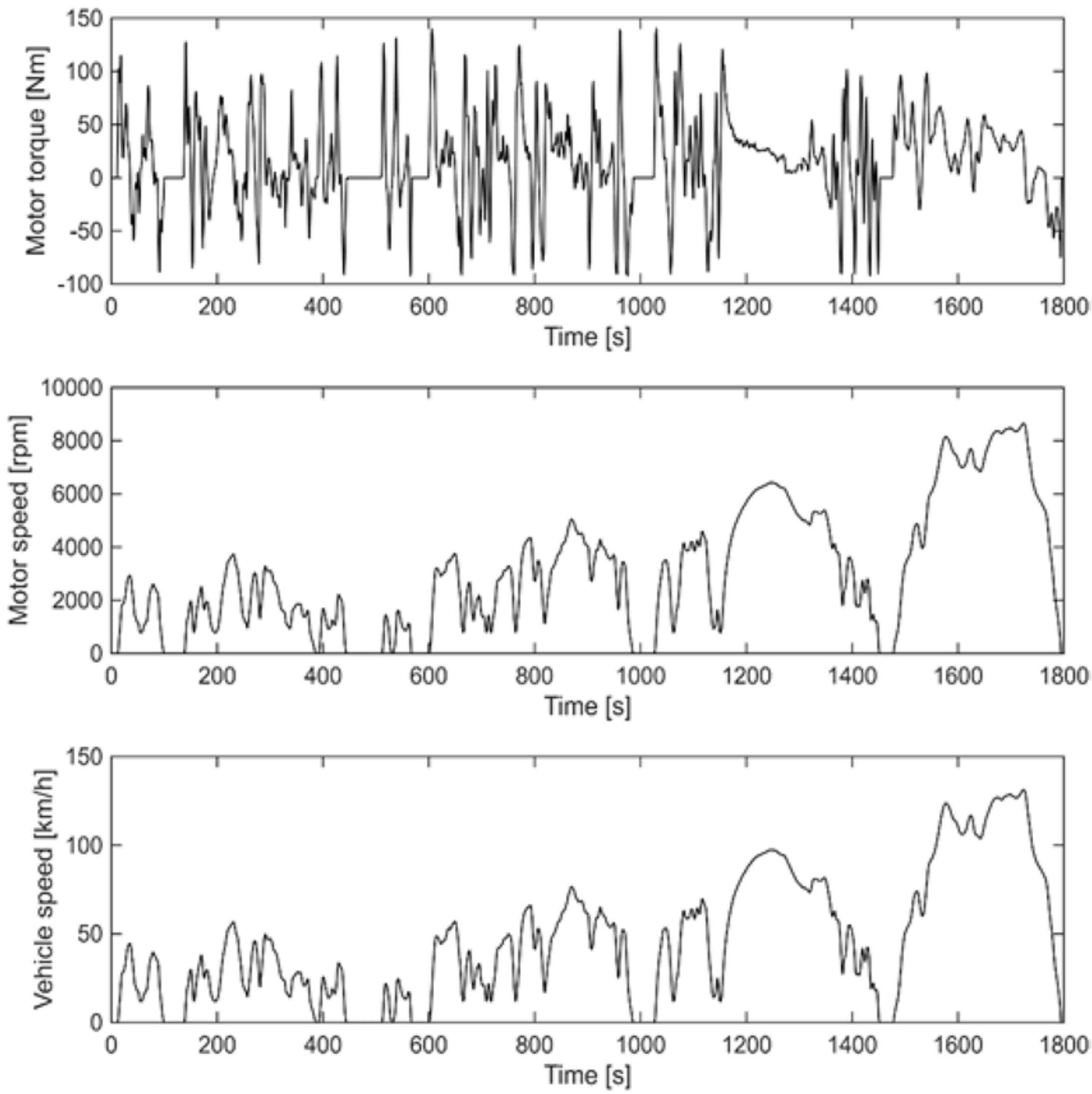

Fig. 3. Powertrain operating conditions following the WLTC class 3 driving cycle.

and the fraction of scenarios exhibiting at least one susceptible gear mesh is:

$$F_G = \frac{1}{N}\sum_{k=1}^{N} G(k) \tag{6}$$

Let $\mathscr{G}$ to be the set of admissible discharge grounds (e.g., A,C,D,E,F,G,H,M) as defined by the network topology in Fig. 5. For each ground $g \in \mathscr{G}$, the network defines at least one admissible path, P, from the source node to ground, g. In the specific simplified resistive arrangement used in this work, the topology is radial, so each g is associated with a unique path, $P(g)$.

Each path is composed of shaft segments $j \in P(g)$ with resistances $R_{s,j}$, and lubricated contacts $i \in P(g)$ with resistances $R_i(k)$, including bearing contacts R_b and gear meshes R_z.

To obtain a semi-quantifiable approximation consistent with the same topology (Fig. 5), each lubricated contact is mapped to an equivalent resistance value based on the lubrication regime inferred from λ. The mapping is intentionally order-of-magnitude to reflect the abrupt change in conduction capability between lubrication regimes (boundary (BDY), mixed (MIX) and electrohydrodynamic (EHL)):

$$R_i(k) = \begin{cases} R_{\mathrm{BDY}}, & \lambda_i(k) < 1 \\ R_{\mathrm{MIX}}, & 1 \le \lambda_i(k) < 3 \\ R_{\mathrm{EHL}}, & \lambda_i(k) \ge 3 \end{cases} \tag{7}$$

In the calculations reported in this work, the following magnitudes are used:

$$R_{\mathrm{BDY}} = 10^3\,\Omega,\ R_{\mathrm{MIX}} = 10^6\,\Omega,\ R_{\mathrm{EHL}} = 10^9\,\Omega \tag{8}$$

It should be noted that these resistance values are not intended to represent universal or exact contact resistances, but rather simplified order-of-magnitude estimates assigned to capture the relative transition in conductive behavior across different lubrication regimes. This approach provides a first methodological demonstration of the proposed CSS framework. The selected magnitudes are consistent with electrical contact resistance (ECR) ranges reported in the literature for lubricated contacts under metallic interaction, tribofilm formation, and insulating interfacial conditions [27]. In this sense, the framework remains flexible, allowing the use of experimentally measured or application-specific contact resistance values in future implementations.

Shaft segment resistances $R_{s,j}$ are assigned a small finite value consistent with steel conduction, such that they remain negligible compared to contact impedances while enabling equivalent-resistance

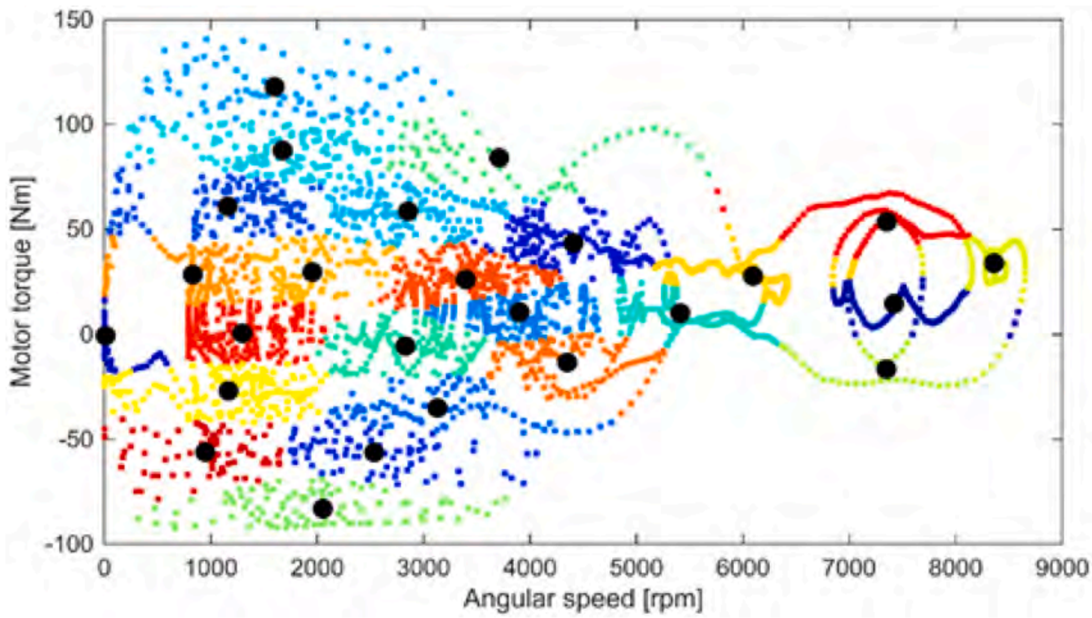

Fig. 4. Most representative operating points in the torque–speed plane (black dots). These points are the geometric centroids of the clusters represented by colored dots, identified through *k*-means.

Table 1
Data from the selected critical scenarios (torque–speed points) for the study.

Electric motor operating scenario	Input speed [rpm]	Torque [Nm]	Duty [%]
1	7422	14.36	2
2	10	-0.51	14
3	4409	43.39	4
4	2537	-56.34	3
5	1160	60.88	3
6	3130	-34.96	3
7	3902	10.55	6
8	1602	117.92	2
9	2853	58.53	4
10	1675	87.61	4
11	5411	10.01	5
12	2830	-5.52	4
13	3713	84.08	2
14	2055	-83.11	3
15	7348	-16.59	1
16	8359	33.71	4
17	1166	-26.93	4
18	6099	27.65	6
19	1955	29.58	3
20	833	28.30	3
21	4348	-13.32	3
22	3398	25.98	7
23	1295	0.67	7
24	7355	53.64	3
25	949	-56.08	2

computations:

$$R_{s,j} = 10^{-5}\,\Omega \tag{9}$$

This assignment preserves the physical ordering $R_s \ll R_b, R_z$ while avoiding the numerical singularity of ideal zero-resistance segments.

For each ground g, the equivalent resistance of its unique path $P(g)$ at operating point k is computed as the series sum of shaft and contact resistances:

$$R_{\text{path},g}(k) = \sum_{j\in P(g)} R_{s,j} + \sum_{i\in P(g)} R_i(k) \tag{10}$$

The predicted dominant discharge ground (ground landing) is then obtained by selecting the minimum path resistance:

$$g^*(k) = \arg\min_{g\in\mathcal{G}} R_{\text{path},g}(k) \tag{11}$$

According to the resistive arrangement, then we have the following path resistances for each ground:

$$\text{A}: \ R_{s1} + R_{b1} \tag{12}$$

$$\text{C}: R_{s2} + R_{b2} \tag{13}$$

$$\text{D}: R_{s2} + R_{s3} + R_{b3} \tag{14}$$

$$\text{E}: \ R_{s2} + R_{s3} + R_{s4} + R_{s5} + R_{b4} \tag{15}$$

$$\text{F}: \ R_{s2} + R_{s3} + R_{s6} + R_{z1z2} + R_{b5} \tag{16}$$

$$\text{G}: \ R_{s2} + R_{s3} + R_{s7} + R_{s8} + R_{z1z2} + R_{b6} \tag{17}$$

$$\text{H}: \ R_{s2} + R_{s3} + R_{s7} + R_{s9} + R_{z1z2} + R_{z3z4} + R_{b7} \tag{18}$$

$$\text{M}: \ R_{s2} + R_{s3} + R_{s7} + R_{s10} + R_{z1z2} + R_{z3z4} + R_{b8} \tag{19}$$

This provides a direct, quantifiable criterion for discharge-ground estimation that remains consistent with the Lambda ratio-driven resistance assignment.

Although the CSS framework is not intended to predict absolute current magnitude, a relative "current share" metric can be estimated by modeling all ground paths as parallel branches driven by the same source node. The branch conductance is:

$$Y_g(k) = \frac{1}{R_{\text{path},g}(k)} \tag{20}$$

and the normalized fraction of current flowing through each ground branch is approximated as:

$$\eta_g(k) = \frac{Y_g(k)}{\sum_{m\in\mathcal{G}} Y_m(k)} = \frac{1/R_{\text{path},g}(k)}{\sum_{m\in\mathcal{G}} 1/R_{\text{path},m}(k)} \tag{21}$$

The parameter $\eta_g(k)$ allows the ranking of grounds not only by the most likely landing point, but also by their relative propensity to carry leakage current. This current fraction corresponds to the relative share of leakage current that may be expected to flow through each conductive

Table 2
KISSsoft input parameters for EHL modelling of the drivetrain's bearings and gear meshes.

Category	Parameter	Value
Software	KISSsoft version	Release 2025
Gear Geometry	Module	2.5 mm
	Number of teeth	$z_1 = 26$
		$z_2 = 61$
		$z_3 = 24$
		$z_4 = 88$
	Pressure angle	18° (z_1z_2)
		20° (z_3z_4)
	Helix angle	29° (z_1z_2)
		19° (z_3z_4)
	Face width	31 mm (z_1)
		29 mm (z_2)
		40 mm (z_3)
		38 mm (z_4)
	Profile shift coefficient	0.3810 (z_1)
		0.1330 (z_2)
		0.4483 (z_3)
		0.4446 (z_4)
Gear Material (18CrNiMo7-6)	Young's modulus	206 GPa
	Poisson's ratio	0.3
	Surface hardness	61 HRC
Bearing Data	Bearing type	Deep groove ball bearing (b_1 to b_6)
		Tapered roller bearing (b_7 and b_8)
	Bearing reference/series	SKF 6210 (b_1 and b_5)
		SKF 6310 (b_2)
		SKF 6209 (b_3)
		FAG 6209 (b_4)
		SKF 6210-ZNR (b_6)
		SKF 32916 (b_7 and b_8)
	Internal clearance class	Normal (CN)
Surface Roughness, R_q	Driving gear	0.3 μm (Case 1)
		0.1 μm (Case 2)
	Driven gear	0.3 μm (Case 1)
		0.1 μm (Case 2)
	Bearing rolling element	0.1 μm
	Bearing raceway	0.1 μm
Lubricant Properties	Lubricant type	Mineral oil
	ISO viscosity grade	ISO-VG 46
	Density	878 kg/m^3
	Kinematic viscosity at operating temperature	17.8 mm^2/s
	Operating oil temperature	70°C
Modeling Assumptions	Lubrication type	Oil bath
	Thermal model	Constant temperature
	Starvation effects	Neglected

path of the drivetrain network. It is calculated from the normalized conductance of each path and provides a probabilistic indicator of the most favorable discharge route, rather than an absolute prediction of current magnitude. By considering the assumption that the drivetrain network behaves as a set of parallel conductive branches connected to a common shaft-voltage source, the normalized conductance of each path reflects its relative likelihood of carrying the leakage current. It should be noted that the calculated current fractions and grounding probabilities are relative susceptibility indicators derived from the assumed resistance hierarchy, and should not be interpreted as absolute electrical probabilities. Their primary purpose is to rank the most favorable conductive paths under varying lubrication conditions.

Let the fraction of current flowing through the path leading to ground, g, at the operating scenario, k, be denoted as $\eta_g(k)$, as defined previously. Considering that all admissible current paths are included in the normalization, the sum of the fractions satisfies:

$$\sum_{g\in G}\eta_g(k) = 1 \tag{22}$$

where G denotes the set of all possible grounding locations in the drivetrain network.

The probability that the leakage current passes through a given gear mesh may be estimated by summing the current fractions of all paths. It involves that interface since each grounding path contains a specific set of mechanical interfaces.

In the simplified drivetrain topology, the gear mesh z_1z_2 is included in the conductive paths leading to the grounds F, G, H, and M. The probability that the leakage current propagates through this gear mesh for operating scenario, k, is defined as:

$$P_{z_1z_2}(k) = \eta_F(k) + \eta_G(k) + \eta_H(k) + \eta_M(k) \tag{23}$$

In a similar way, the gear mesh z_3z_4 is included only in the paths leading to the grounds H and M. The corresponding probability becomes:

$$P_{z_3z_4}(k) = \eta_H(k) + \eta_M(k) \tag{24}$$

Because the topology of the drivetrain requires the current to pass through z_1z_2 before reaching z_3z_4, any current flowing through the latter necessarily traverses both meshes. The probability of simultaneous conduction through both gear meshes is:

$$P_{z_1z_2\cap z_3z_4}(k) = \eta_H(k) + \eta_M(k) \tag{25}$$

These probabilities represent scenario-dependent conductive susceptibility indicators rather than statistical probabilities derived from repeated calculations. Additionally, to account for real operating conditions through the duty-cycle, a usage factor u_k is then introduced to represent the fraction of time associated with each operating scenario:

$$u_k \geq 0, \sum_{k=1}^{N} u_k = 1 \tag{26}$$

Using this factor, the CSS outputs can be aggregated into duty-cycle-representative indicators. Therefore, the duty-cycle weighted probability of current propagation through gear mesh z_1z_2 becomes:

$$\bar{P}_{z_1z_2} = \sum_{k=1}^{N} u_k P_{z_1z_2}(k) \tag{27}$$

the weighted probability for gear mesh z_3z_4 may be:

$$\bar{P}_{z_3z_4} = \sum_{k=1}^{N} u_k P_{z_3z_4}(k) \tag{28}$$

and the weighted current fraction associated with ground g can be:

$$\bar{\eta}_g = \sum_{k=1}^{N} u_k \eta_g(k) \tag{29}$$

These weighted indicators suggest an operation-representative evaluation of drivetrain conductive susceptibility and may serve as prognostic indicators of potential gear-current propagation under realistic operating conditions.

3. Results

Fig. 6 shows the scenario-resolved dominant conductive paths and associated grounding locations predicted by the CSS methodology for the 25 representative operating scenarios. The minimum film thickness and Lambda ratios obtained for both Case 1 and Case 2 are fully provided in Tables A1-A4 in the supplementary material. The results in Fig. 6 show evidence that the predicted grounding location varies with operating conditions as expected, indicating that leakage-current discharge in the drivetrain is strongly dependent on the instantaneous torque–speed state. The lubrication regime of bearings and gear meshes also evolves as the operating conditions change, modifying the electrical resistance assigned to each interface. This leads to changes in the equivalent resistance of the conductive paths and different preferred

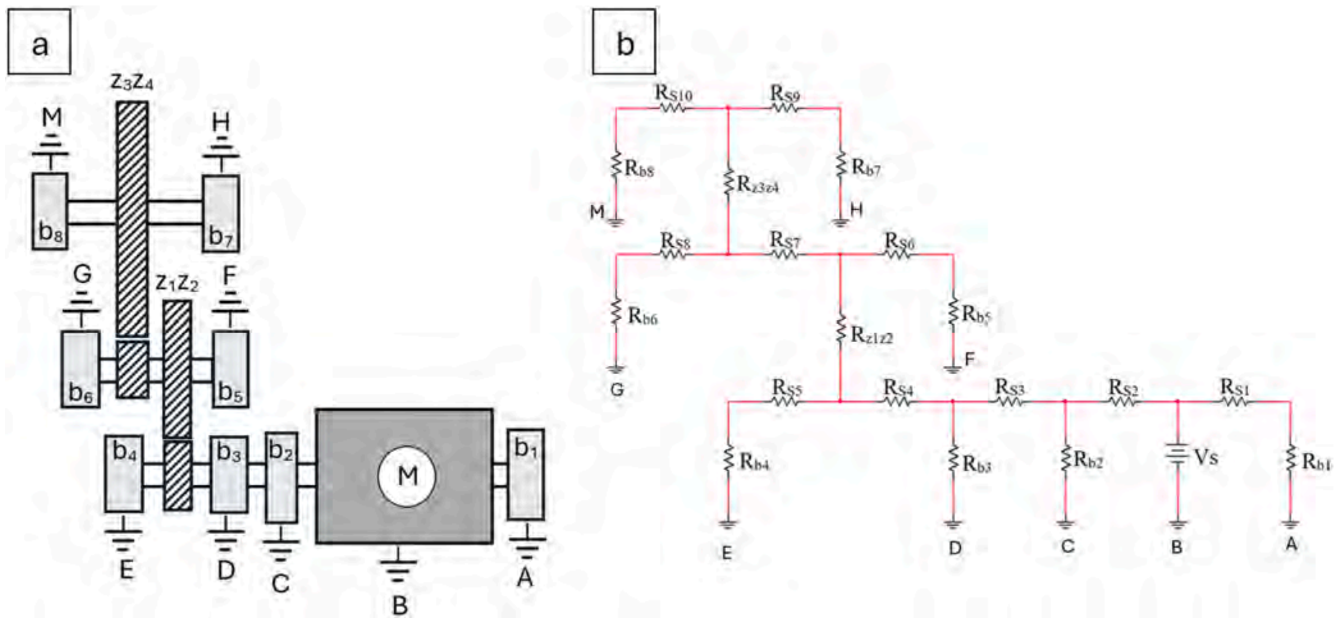

Fig. 5. (a) Simplified mechanical diagram of the drivetrain system showing the motor (M), two gear pairs (z_1z_2, $|z_3z_4$), and the supporting bearings b_1--b_8 connected to the housing through nodes $A--M$. (b) Equivalent resistive-simplified electric diagram analog of the mechanical system, where the resistances $R_{s1}--R_{s10}$ represent shafts resistances, $R_{b1}--R_{b8}$ resistances of bearings' lubricated contacts, $R_{z1z2}$and R_{z3z4} represent the resistances of lubricated gear-mesh interactions, and V_s corresponds to the DC voltage excitation from the motor.

grounding locations. Consequently, no single grounding point dominates across the entire operating envelope while several discharge nodes become active depending on the operating scenario.

The comparison between Case 1 and Case 2 reveals that the predicted grounding paths are very sensitive to bearing and gear surface roughness situation. In Case 1, where gear surfaces have higher roughness than bearings, gear meshes tend to operate with lower Lambda ratios, which increases their conductive susceptibility and promotes grounding paths that propagate through the gear stages. In contrast, in Case 2, the more uniform gear surface roughness conditions increase the lubrication separation in the gear meshes, leading in several scenarios to alternative conductive routes that involve different drivetrain interfaces. As a result, some operating scenarios exhibit changes in the dominant grounding location between the two cases, highlighting the influence of tribological parameters on the electrical connectivity of the drivetrain.

Fig. 7 shows the duty-cycle weighted probability (%) of the dominant conductive path landing at each grounding location in the drivetrain for the two surface roughness situations. The percentages indicate the probability that the dominant conductive path ends at the corresponding bearing location over the complete driving cycle.

In Case 1, the highest grounding probabilities occur at M (b8) and H (b7), each accounting for 32.9% of the events, indicating that leakage-current discharge is most likely to occur at the bearings supporting the upper shaft. Secondary contributions appear at G (b6) and F (b5) (~10.5%), while the remaining bearings exhibit relatively small probabilities (~3.3%). This distribution reflects the increased conductive susceptibility of the gear meshes under higher gear roughness conditions, facilitating discharge paths closer to the motor side of the drivetrain.

In Case 2, the grounding distribution shifts toward the output-side bearings. The highest probability occurs at E (b4) (25.9%), followed by D (b3) (17.3%) and C (b2) and A (b1) (14.7%). On the other hand, the motor-side bearings M (b8) and H (b7) showed significantly lower probabilities (5.5%). This shift indicates that improved lubrication separation at the gear meshes enabled a reduction of their conductive role, which allows the conductive paths toward downstream bearings to become dominant.

4. Discussion

4.1. Case 1: Effect of different surface roughness in bearings and gears

Figs. 8a-c show three complementary representations that illustrate how gear-current susceptibility varies across operating conditions and over the complete driving cycle for Case 1 (where gears exhibit higher surface roughness than bearings). Fig. 8a classifies the operating conditions according to the dominant current propagation path within the drivetrain. Most operating points fall within the gear current region, indicating that leakage-current propagation frequently involves at least one gear mesh. In particular, several operating conditions show dominant propagation through both gear meshes **(**z_1z_2 and z_3z_4**)**, while others are dominated by conduction through the first gear mesh (z_1z_2). Only a limited number of scenarios fall within the no-gear current region or bearing current region, which is primarily associated with high-speed conditions. At these speeds, the increase in lubricant film thickness leads to higher lambda ratios and improved electrical insulation of the gear contacts, making alternative conductive paths through bearings more favorable.

The duty-cycle weighted probabilities of gear conduction are shown in Fig. 8b. These results demonstrate that propagation through the z_1z_2 gear mesh dominates, exhibiting a probability close to 90%, while propagation through both gear meshes occurred with a probability of 60–65%. In contrast, the probability of current bypassing the gears is relatively low. It confirms that gear contacts play a critical role in the conductive network under the roughness conditions considered in this case. Fig. 8c shows the scenario-resolved probability distribution of gear-current propagation for the 25 representative operating scenarios. Many scenarios exhibited a high chance of current propagation through at least one gear mesh, in particular for moderate speed and loading conditions. Several operating points displayed near-certain propagation through both gear meshes while only a small number of high-speed scenarios show a significant probability of non-gear conductive paths.

4.2. Case 2: Effect of similar surface roughness in bearings and gears

Fig. 9a shows a classification of the operating conditions according to

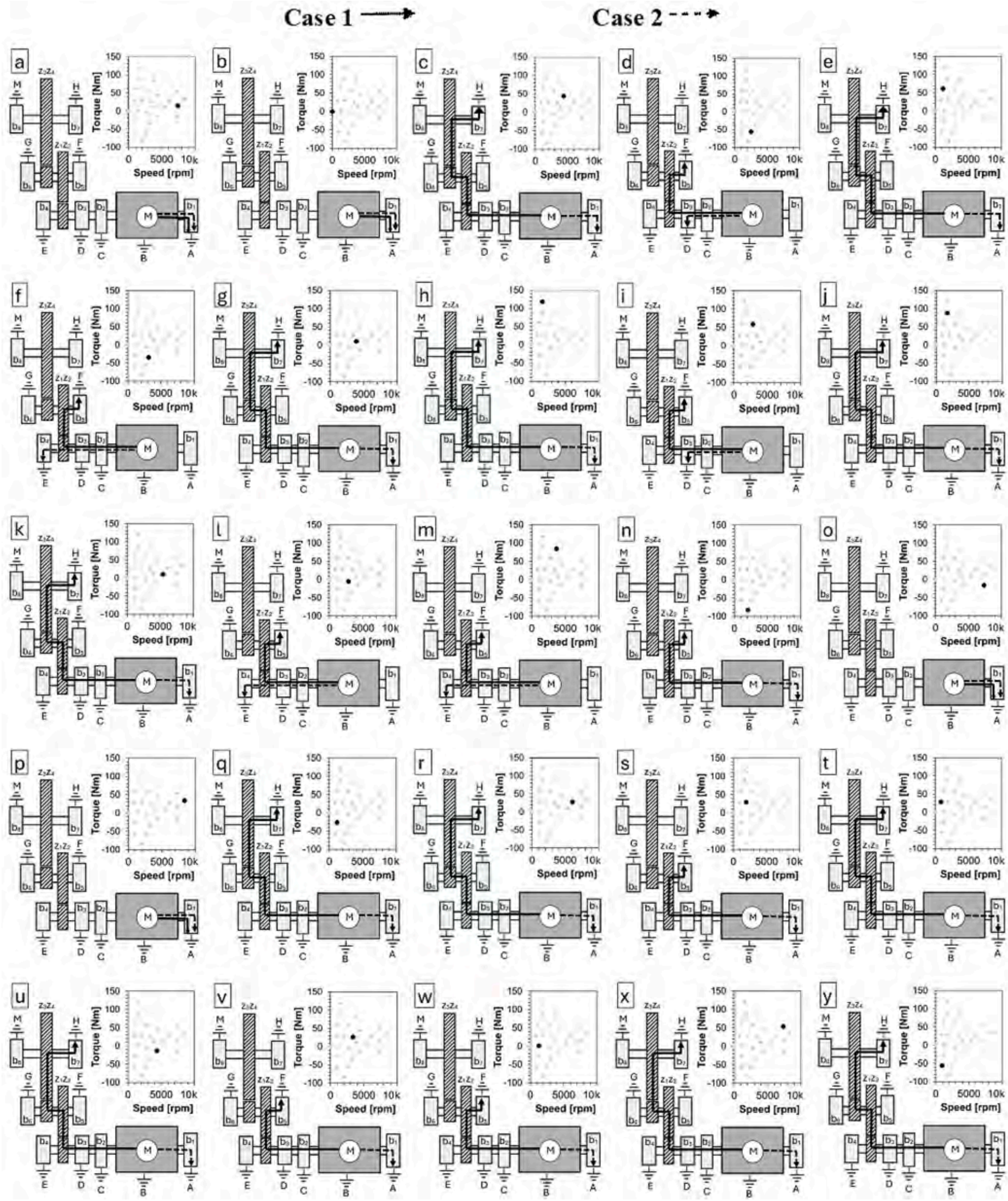

Fig. 6. Identification of conductive paths within the drivetrain using the CSS methodology for Case 1 and Case 2. Each panel (a–y) corresponds to one operating scenario defined by a specific speed–torque condition (shown in the inset plots). The highlighted black/continuous arrows indicate the predicted dominant conductive path through the drivetrain for Case 1. The highlighted black/strip arrows indicate the predicted dominant conductive path through the drivetrain for Case 2. The black marker in each speed–torque map shows the evaluated operating point within the full operating envelope.

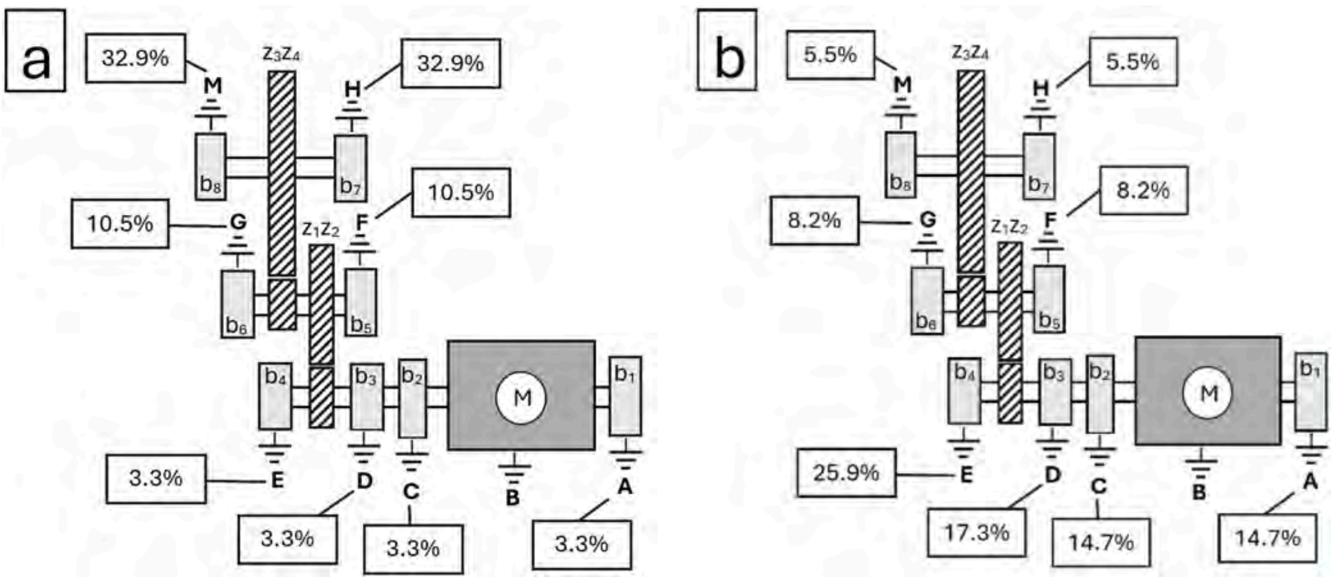

Fig. 7. Duty-cycle weighted probability distribution of the dominant conductive path across the drivetrain grounding locations predicted by the CSS methodology for: (a) Case 1; and (b) Case 2.

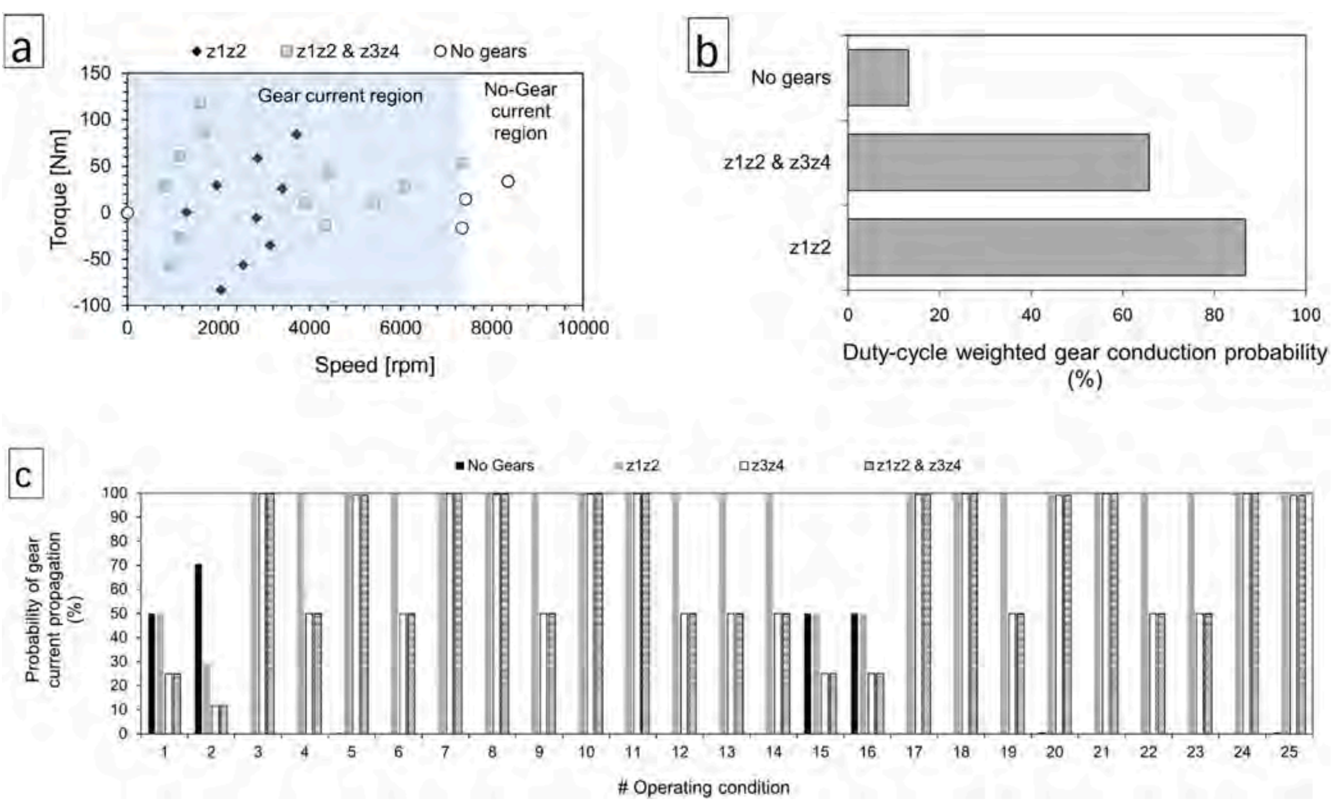

Fig. 8. Results showing the probability of leakage current propagation through gear meshes for Case 1: (a) Operating conditions grouped by the predicted dominant current path through the drivetrain gear meshes; (b) Duty-cycle-weighted conduction probability for each gear mesh; (c) Duty-cycle-weighted probability of gear-current propagation under each operating condition, indicating the likelihood of current flowing through gear meshes z_1z_2, z_3z_4, both meshes, or through non-gear paths.

the dominant current propagation path. In contrast to Case 1, all operating points fall within the no-gear current region, indicating that the dominant conductive path does not involve the gear meshes for any of the evaluated operating scenarios. In fact, current propagation is likely to occur through bearings (bearing currents). This behavior results from the improved lubrication separation of the gear contacts under the assumed surface conditions, which increases the Lambda ratio and consequently the electrical resistance of the gear meshes. The duty-cycle aggregated results shown in Fig. 9b confirm this trend. The probability of non-gear conductive paths dominates the driving cycle, reaching approximately 70–75%, while the probability of current propagation through the z_1z_2 mesh is significantly lower (around 25–30%). The likelihood of propagation through both gear meshes remains comparatively small. These results suggest that, under the smoother surface conditions assumed in Case 2, gear contacts rarely constitute the most favorable conductive route within the drivetrain network. In addition,

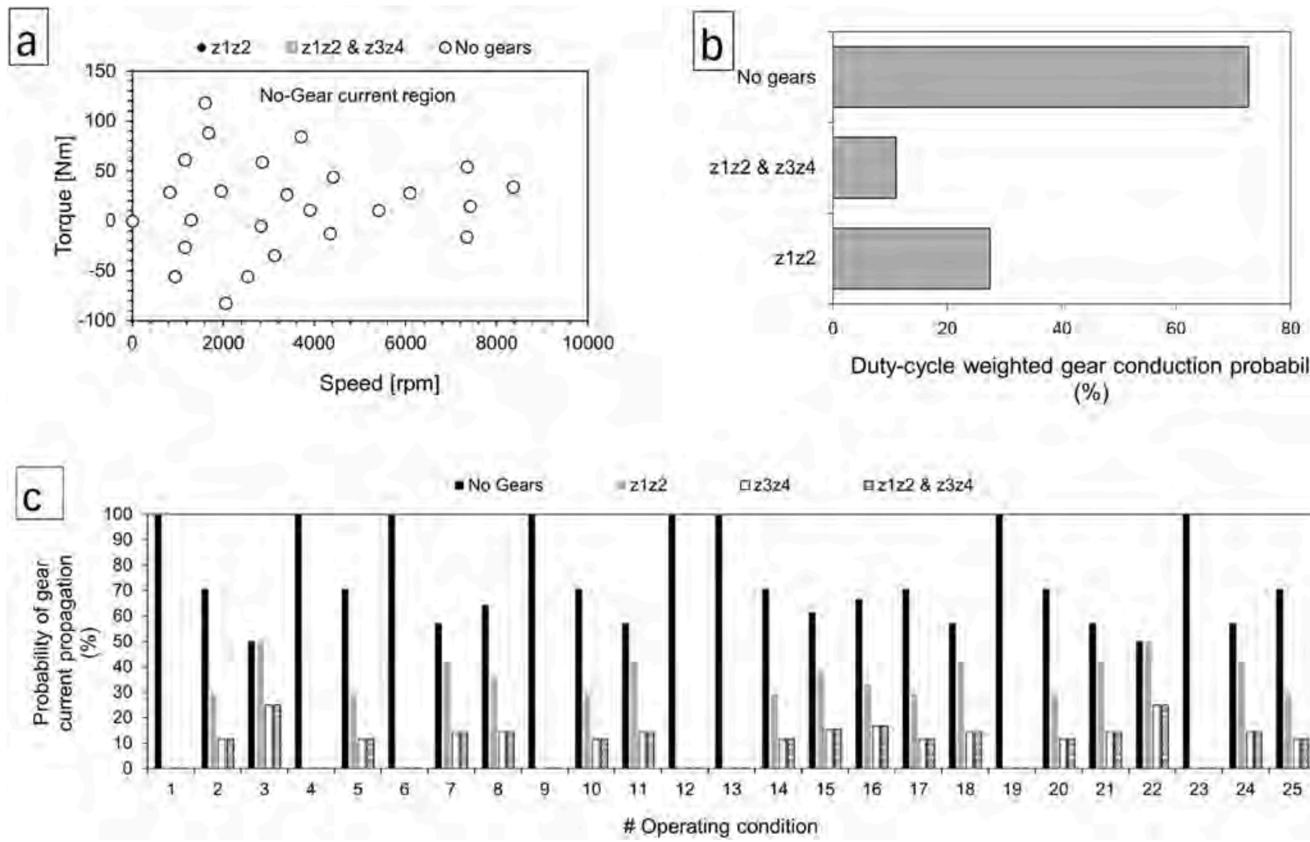

Fig. 9. Results showing the probability of leakage current propagation through gear meshes for Case 2: (a) Operating conditions grouped by the predicted dominant current path through the drivetrain gear meshes; (b) Duty-cycle-weighted conduction probability for each gear mesh; (c) Duty-cycle-weighted probability of gear-current propagation under each operating condition, indicating the likelihood of current flowing through gear meshes z_1–z_2, z_3–z_4, both meshes, or through non-gear paths.

Fig. 9c presents the scenario-resolved probability distribution of gear-current propagation. The results show that most operating conditions exhibit a very high probability of non-gear current propagation, often approaching or exceeding 90%. Although small probabilities of conduction through the gear meshes are still predicted for some scenarios, these contributions are secondary compared with the dominant conductive paths through bearings.

Overall, comparing Case 1 and Case 2 clearly shows how important surface roughness is in shaping the current propagation in an EV drivetrain. Gear meshes can move from being key conductive paths to playing a much smaller role, depending on surface conditions, which highlights surface roughness as one of the most critical design factors that can be considered to prevent stray currents-driven risk of failures in EV drivetrains. One implication of these results is that modifying local conductive susceptibility may redistribute leakage-current paths across the drivetrain. While this may shift electro-tribological damage from one component to another, such redistribution can also be exploited strategically. By identifying the most probable conductive routes, grounding brushes or sacrificial elements may be intentionally placed to control where current discharge occurs, concentrating damage on components that are easier or less costly to replace. This highlights the value of evaluating conductive-path optimization from a total drivetrain reliability and maintenance perspective. Besides, although EV-dedicated e-fluids may present lower viscosities and different electrical properties, the proposed framework can be transferable to other lubricants by updating the lubricant rheological and electrical parameters accordingly in the EHL simulation software.

It should be noted that, unlike bearing-current studies widely available in the literature, no previous system-level predictive methodologies integrating gear-mesh conductive susceptibility under transient EV operating conditions have been reported. Therefore, the present results should be interpreted as a first methodological benchmark for future developments in this area and valuable in early drivetrain design stages to anticipate potential failure risks.

5. Conclusions

It was possible to have a first insight into the conductive susceptibility of EV drivetrains through this pioneer framework, in particular, to understand how leakage currents can propagate not only through bearings, but also through gear meshes. Using EHL simulations and a simplified electrical representation, the proposed conductive susceptibility scheme (CSS) provided a practical and physically meaningful way to analyze conductive paths at the system level of an EV driveline by combining realistic driving conditions. According to the findings, the following conclusions were drawn:

- The results showed that conductive pathways in EV drivetrains are highly dynamic and influenced by the operating conditions. Changes in torque and speed affect the lubrication regime of each tribological contact, promoting alterations in its electrical resistance. Consequently, leakage-current paths were not fixed, but shifted across the drivetrain depending on the instantaneous operating state.
- Gear meshes can become active conductive elements in EV drivetrains depending on their lubrication state. While the influence of surface roughness on local conductive susceptibility is expected from tribological principles, the CSS framework revealed how these local changes affect the formation and redistribution of dominant leakage-current paths at the drivetrain level.

- Smoother gear surfaces promoted greater lubrication separation and reduced the conductive participation of gear meshes, shifting the dominant current paths toward bearings. This demonstrates how tribological parameters can modify the system-level conductive susceptibility distribution in EV transmissions.
- The CSS framework provides a predictive tool for early-stage conductive path mapping and ranking in EV drivetrains. Although it does not aim to predict exact current magnitudes, it captures the relative evolution of conductive pathways and offers insight into how operating and tribological conditions shape electro-tribological interactions at the system level.
- Overall, this study highlighted the need to move beyond a purely bearing-focused view of stray-current phenomena and to consider the full drivetrain as an interconnected electro-tribological system. In this context, gear meshes should not be overlooked, as they can play a significant role in current propagation and, ultimately, in drivetrain reliability.

Declaration of generative AI and AI-assisted technologies in the writing process

During the preparation of this work the authors used ChatGPT in order to improve clarity and readability of the manuscript. After using these services, the authors reviewed and edited the content as needed and take full responsibility for the content of the published article.

CRediT authorship contribution statement

Leonardo I. Farfan-Cabrera: Writing – review & editing, Writing – original draft, Visualization, Project administration, Methodology, Investigation, Data curation, Funding acquisition, Formal analysis, Conceptualization. **Renato Galluzzi:** Writing – review & editing, Validation, Investigation, Formal analysis, Software, Data curation. **Andys Hernández-Peña:** Writing – review & editing, Validation, Methodology, Formal analysis. **Thomas Tobie:** Writing – review & editing, Formal analysis, Conceptualization.

Declaration of competing interest

The authors declare that they have no known competing financial interests or personal relationships that could have appeared to influence the work reported in this paper.

Acknowledgments

L.I.F.-C., R.G. and A.H.-P. acknowledge the financial support given by Tecnologico de Monterrey within the Challenge-based research project IJST070-23EG68001 (call 2023) for conducting this research.

Supplementary materials

Supplementary material associated with this article can be found, in the online version, at doi:10.1016/j.rineng.2026.111934.

Data availability

Data will be made available on request.

References

[1] L.I. Farfan Cabrera, P. Lee, A. Erdemir (Eds.), Electric vehicle fluid testing, CRC Press, 2026.
[2] L.I. Farfan-Cabrera, A. Erdemir (Eds.), Electric vehicle tribology: Challenges and opportunities for a sustainable transportation future., Elsevier., 2024.
[3] D. Berman, L.I. Farfan-Cabrera, A. Rosenkranz, A. Erdemir, Advancing the frontiers of ev tribology with 2D materials – a critical perspective, Materials Science and Engineering: R: Reports 161 (2024) 100855, https://doi.org/10.1016/j.mser.2024.100855.
[4] F. Xu, N. Ding, N. Li, L. Liu, N. Hou, N. Xu, W. Guo, L. Tian, H. Xu, C.-M.L. Wu, X. Wu, X. Chen, A review of bearing failure modes, mechanisms and causes, Engineering Failure Analysis 152 (2023) 107518, https://doi.org/10.1016/j.engfailanal.2023.107518.
[5] F. He, G. Xie, J. Luo, Electrical bearing failures in electric vehicles, Friction 8 (1) (2020) 4–28, https://doi.org/10.1007/s40544-019-0356-5.
[6] Z. Xiao, M. Hu, S. Chen, K. Cao, Bearing electrical-erosion damage in electrical drive systems: a review, IEEE Transactions on Transportation Electrification 10 (2) (2024) 3428–3442, https://doi.org/10.1109/TTE.2023.3301580.
[7] S. Liu, J. Lv, S. Jiang, L. Kuang, L. Zhao, C. Liu, Correlation between shaft voltage characteristics, electrical discharge behavior and surface damage of motor bearing in ev bench tests, Wear 582–583 (2025) 206344, https://doi.org/10.1016/j.wear.2025.206344.
[8] L. Guo, H. Mol, T. Nijdam, L. de Vries, Investigation of the discharge voltage in electric vehicle motor bearings, Tribology Transactions 67 (6) (2024) 1158–1167, https://doi.org/10.1080/10402004.2024.2419450.
[9] L. Guo, H. Mol, T. Nijdam, L. de Vries, J. Bongaerts, Study on the electric discharge behaviour of a single contact in ev motor bearings, Tribology International 187 (2023) 108743, https://doi.org/10.1016/j.triboint.2023.108743.
[10] R. Lokhande, S.K. Mishra, D. Ronanki, P. Shakya, V. Edachery, L. Koottaparambil, Review on tribological and vibration aspects in mechanical bearings of electric vehicles: effect of bearing current, shaft voltage, and electric discharge material spalling current, Lubricants 13 (8) (2025) 349, https://doi.org/10.3390/lubricants13080349.
[11] T. Hadden, J.W. Jiang, B. Bilgin, Y. Yang, A. Sathyan, H. Dadkhah, A review of shaft voltages and bearing currents in ev and hev motors, in: Proceedings of the 42nd Annual Conference of the IEEE Industrial Electronics Society (IECON 2016), IEEE, 2016, pp. 1–8, https://doi.org/10.1109/IECON.2016.7793357.
[12] S. Syla, K.M. Brill, S. Paulus, S. Graf, O. Koch, A detailed multibody simulation model for ball bearings to predict friction and electrical capacitance, Lubricants 14 (4) (2026) 154, https://doi.org/10.3390/lubricants14040154.
[13] A. Bleger, M. Leighton, N. Morris, Automotive e-motor bearing electrical discharge phenomena: an experimental and numerical investigation, Tribology International 191 (2024) 109140, https://doi.org/10.1016/j.triboint.2023.109140.
[14] L. Houpert, J. Clarke, C. Penny, Tribological models for advanced ball bearing simulation, Tribology Transactions 66 (4) (2023) 645–660, https://doi.org/10.1080/10402004.2023.2213470.
[15] R.L. Jackson, S. Saha, J.R. Janik, A statistical prediction of electrical discharge initiation and semi-analytical transient mixed lubrication model of a rolling element, Journal of Tribology 147 (5) (2025) 051103, https://doi.org/10.1115/1.4066520.
[16] S. Chatterton, P. Pennacchi, A. Vania, Electrical pitting of tilting-pad thrust bearings: modelling and experimental evidence, Tribology International 103 (2016) 475–486, https://doi.org/10.1016/j.triboint.2016.08.003.
[17] A. Gonda, S. Paulus, S. Graf, O. Koch, S. Götz, B. Sauer, Basic experimental and numerical investigations to improve the modeling of the electrical capacitance of rolling bearings, Tribology International 193 (2024) 109354, https://doi.org/10.1016/j.triboint.2024.109354.
[18] L.I. Farfan-Cabrera, Tribology of electric vehicles: a review of critical components, current state and future improvement trends, Tribology International 138 (2019) 473–486, https://doi.org/10.1016/j.triboint.2019.06.029.
[19] G. Du, W. Cao, S. Hu, Z. Lin, T. Yuan, Design and assessment of an electric vehicle powertrain model based on real-world driving and charging cycles, IEEE Transactions on Vehicular Technology 68 (2) (2019) 1178–1187, https://doi.org/10.1109/TVT.2018.2884812.
[20] R.L. Jackson, Modeling electrical resistance of lubricated contacts, in: L.I. Farfan-Cabrera, A. Erdemir (Eds.), Electric vehicle tribology: Challenges and opportunities for a sustainable transportation future, Elsevier, 2024, pp. 207–224, https://doi.org/10.1016/B978-0-443-14074-7.00012-1.
[21] P. Höltje, L. Jünemann, B. Knebusch, N. Euler-Rolle, A. Zeiler, A. Mertens, Prediction and measurement of bearing currents in an electric traction drive system, in: 2023 11th International Conference on Power Electronics and ECCE Asia (ICPE 2023 – ECCE Asia)., IEEE, 2023, https://doi.org/10.23919/ICPE2023-ECCEAsia54778.2023.10213740.
[22] F. Jia, Y. Lei, X. Liu, Y. Fu, J. Hu, Simulation and experimental study on lubrication of high-speed reducer of electric vehicle, Industrial Lubrication and Tribology 73 (3) (2021) 500–507, https://doi.org/10.1108/ILT-08-2020-0309.
[23] N. Rosenberger, et al., Quantifying the state of the art of electric powertrains in battery electric vehicles: Comprehensive analysis of the Tesla Model 3 on the vehicle level, World Electric Vehicle Journal 15 (6) (2024) 268, https://doi.org/10.3390/wevj15060268.
[24] A. Fatemi, N.A.O. Demerdash, T.W. Nehl, D.M. Ionel, Large-scale design optimization of PM machines over a target operating cycle, IEEE Transactions on Industry Applications 52 (5) (2016) 3772–3782, https://doi.org/10.1109/TIA.2016.2563383.
[25] S.E. Miri, M. Azadi, S. Pakdel, Development of a duty cycle with K-means clustering technique for hydraulic steering in an instrumented TIBA vehicle, Transportation Engineering 8 (2022) 100114, https://doi.org/10.1016/j.treng.2022.100114.
[26] I.M. Hutchings, P. Shipway, Tribology: Friction and wear of engineering materials, 2nd ed., Butterworth-Heinemann, 2017.
[27] A. Tonck, J.M. Martin, P. Kapsa, J.M. Georges, Boundary lubrication with anti-wear additives: Study of interface film formation by electrical contact resistance, Tribology International 12 (5) (1979) 209–213, https://doi.org/10.1016/0301-679X(79)90190-7.